AFRL-AFOSR-VA-TR-2016-0338

Tightly Coupled Mechanistic Study of Materials in the Extreme Space Environment

Adrianus Van Duin
PENNSYLVANIA STATE UNIVERSITY

10/11/2016
Final Report

Air Force Research Laboratory
AF Office Of Scientific Research (AFOSR)/ RTA1
Arlington, Virginia 22203
Air Force Materiel Command

REPORT DOCUMENTATION PAGE

Form Approved
OMB No. 0704-0188

1. REPORT DATE *(DD-MM-YYYY)*	2. REPORT TYPE	3. DATES COVERED *(From - To)*
03-11-2016	Final Performance	01 Jul 2011 to 30 Jun 2016

4. TITLE AND SUBTITLE
Tightly Coupled Mechanistic Study of Materials in the Extreme Space Environment

5a. CONTRACT NUMBER

5b. GRANT NUMBER
FA9550-11-1-0158

5c. PROGRAM ELEMENT NUMBER
61102F

6. AUTHOR(S)
Adrianus Van Duin, DEBORAH LEVIN, Krishna Rajan, Mark Lewis, Raymond Sedwick

5d. PROJECT NUMBER

5e. TASK NUMBER

5f. WORK UNIT NUMBER

7. PERFORMING ORGANIZATION NAME(S) AND ADDRESS(ES)
PENNSYLVANIA STATE UNIVERSITY
201 OLD MAIN
UNIVERSITY PARK, PA 16802-1505 US

8. PERFORMING ORGANIZATION REPORT NUMBER

9. SPONSORING/MONITORING AGENCY NAME(S) AND ADDRESS(ES)
AF Office of Scientific Research
875 N. Randolph St. Room 3112
Arlington, VA 22203

10. SPONSOR/MONITOR'S ACRONYM(S)
AFRL/AFOSR RTA1

11. SPONSOR/MONITOR'S REPORT NUMBER(S)
AFRL-AFOSR-VA-TR-2016-0338

12. DISTRIBUTION/AVAILABILITY STATEMENT
A DISTRIBUTION UNLIMITED: PB Public Release

13. SUPPLEMENTARY NOTES

14. ABSTRACT
The Tightly Coupled Mechanistic Study of Materials in the Extreme Space Environment Group has worked to examine spacecraft contamination issues from the perspective of non- equilibrium gas dynamics (Levin), material response at the atomistic level (Rajan), high fidelity gassurface chemistry models (van Duin), and experiments to characterize and test spacecraft material damage by small source ion bombardment (Sedwick). The goals of the group have been ambitious given the multi-length and time-scale facets that make this problem tremendously challenging. The length scales of contamination vary by probably twelve orders of magnitude and the variation in time scales is similar. The group has had a number of successes, described in 43 journal and conference papers that have been published or are in progress. We established collaborations across length scales, ranging from the smallest (Angstroms) to the largest scales. As such, significant progress was made in the development of computational and experimental collaborative frameworks suitable for predicting the spacecraft environment for new propellants and spacecraft materials.

15. SUBJECT TERMS
Study of Materials, Extreme Environment

16. SECURITY CLASSIFICATION OF:			17. LIMITATION OF ABSTRACT	18. NUMBER OF

a. REPORT	b. ABSTRACT	c. THIS PAGE		PAGES	19a. NAME OF RESPONSIBLE PERSON
Unclassified	Unclassified	Unclassified	UU		BIRKAN, MITAT
					19b. TELEPHONE NUMBER *(Include area code)* 703-696-7234

Final report for AFOSR Grant FA9550-11-1-0158 ending 30 Jun 2016

Introduction.
The Tightly Coupled Mechanistic Study of Materials in the Extreme Space Environment Group has worked to examine spacecraft contamination issues from the perspective of non- equilibrium gas dynamics (Levin), material response at the atomistic level (Rajan), high fidelity gas-surface chemistry models (van Duin), and experiments to characterize and test spacecraft material damage by small source ion bombardment (Sedwick). The goals of the group have been ambitious given the multi-length and time-scale facets that make this problem tremendously challenging. The length scales of contamination vary by probably twelve orders of magnitude and the variation in time scales is similar. As such, the group has had a number of successes which are highlighted in the pages that follow. 43 journal and conference papers have been published or are in progress, resulting from the collaborations across length scales, ranging from the smallest (Angstroms) to the largest scales. As such, significant progress was made in the development of computational and experimental collaborative frameworks suitable for predicting the spacecraft environment for new propellants and spacecraft materials. The sections below describe the specific progress in each of the four groups.

Levin group. Our work under this grant has been focused on understanding the nature of spacecraft contamination from small chemical and electric propulsion thrusters in the extreme environment created by low to mid-orbit space. In this final progress report, we focus on our modeling of charge-exchange (CEX) ions formed through collisions of beam ions with propellant neutral species and the ambient background (space or chamber) since these are the main source of spacecraft contamination. DSMC - particle-in-cell (PIC) models have been developed by numerous researchers, but, the computer technology used to develop these codes does not take advantage of the massively parallel computing environment that exists today at the peta-scale level. Furthermore, it is commonly assumed that CEX may be modeled in an "overlay" manner, i.e., meaning that the any CEX created ions do not significantly affect the plume neutral gas species. [1,2] In fact we observe a difference of 15% in the downstream plume between the velocity profiles of neutral species modeled with and without the inclusion of CEX collisions [3,4] and believe that this difference will be important in understanding the interface between the plasma sheath and spacecraft materials.

We have developed a three-dimensional DSMC simulation tool using the novel grid approach known as a Adaptive Mesh Refinement (AMR) / Octree. [4,5] The computational tool entitled SUGAR, "Scalable Unstructured Gas dynamics with Adaptive Mesh Refinement" is three-dimensional. By employing species-dependent time-steps for ions and neutrals we are able to directly couple the modeling of charge exchange (CEX) reactions to neutral and ion transport, which can have a significant effect on both the ion and neutral velocity fields. Comparison of three-dimensional four thruster neutral plume computations performed using this approach versus the older two-level Cartesian adaption approach [6] demonstrated that the most expensive DSMC

numerical parameter, i.e., the number of computational particles and collision cells, could be reduced by almost an order of magnitude and a factor of approximately 50, respectively. Parallelization speed ups for over 1,000 cores of approximately 80% of ideal have been achieved to date. Recent results for two ion thruster geometries, shown in Fig. 1, will be discussed below.

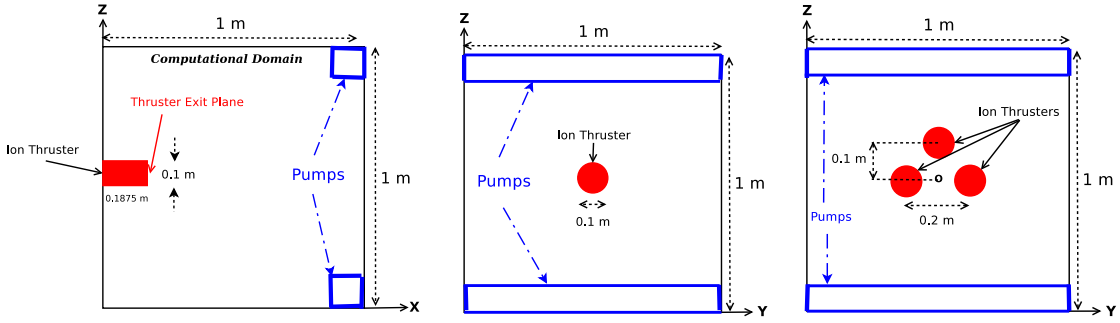

Figure 1.1. Computational domains for single and triple ion thruster configurations for chamber and space boundary condition. Single thruster x-z and y-z planes (LHS and middle, respectively) and triple thruster, y-z plane, RHS.

Figure 2 shows recent examples obtained with the SUGAR DSMC/PIC code. The top two figures (a and b) show the difference in the CEX distribution in a ground chamber compared to the space environment for a single thruster geometry. In the vacuum case, one can observe that the CEX ion population is greatest near the thruster exit, reaching a value of approximately 10% of the total ion number density. This is expected since the densities of neutrals and ions and therefore the collision frequency is highest in this region. The bottom two portions of the figure (c and d) shows a comparison of predicted CEX ion spatial distribution in a ground facility for two wall models. The baseline wall model, assuming that every ion that strikes the wall is neutralized, is the typical engineering assumption. However, even if only 10% of the collisions preserve the ion and its velocity the spatial energy distribution of CEX ions formed in the chamber will be different (see the pink square "collecting region" in Fig. 2c). The AMR-Octree approach was able to resolve the one out of 10,000 beam ion particles that reflect specularly with the wall and arrive at the pink square with less energy than in the baseline case. We are in the process of adding an atomic oxygen species dedicated time step so that we will be able to simultaneously model the "chemical" as well as "ion" species bombardment, both of which are important in the space environment but are currently treated as uncoupled mechanisms.

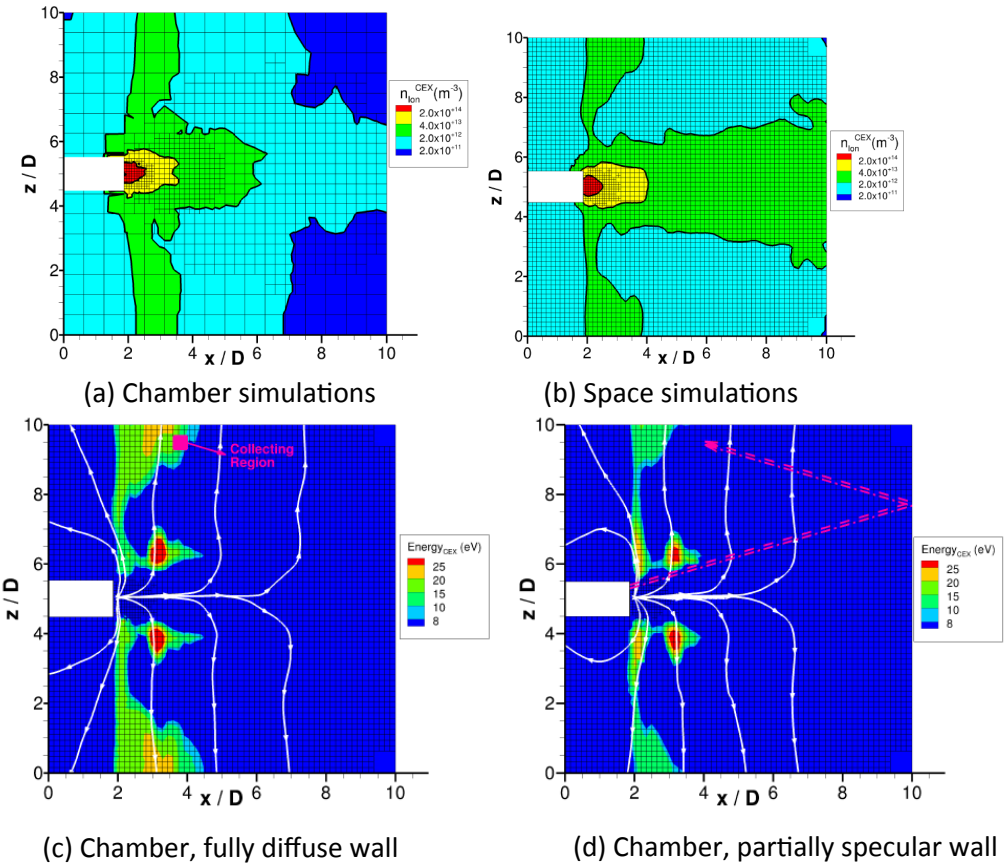

Fig. 1.2 Multi-scale resolution of CEX ion spatial distribution and streamlines for different background gas conditions and wall models. [5]

Turning to the triple thruster geometry, the most obvious change in the neutral and ion number density fields of the triple versus the single thruster case is the asymmetry of the flow which is caused by the interaction of the plumes with each other (see Fig. 3a). A very interesting difference can be observed in the CEX ion distribution between the single and triple thruster cases. Compared to a single thruster, a large change can be observed in Fig. 4a in the spatial region where the 2.0×10^{14} m^{-3} level has significantly expanded because of the increase in the background neutral number density. Moreover, a comparison between chamber (Fig. 4a) and vacuum (Fig. 4b) solutions shows that although an asymmetry is present for the vacuum CEX ion distribution due to plume interactions, the magnitude of the CEX ion population for the chamber case is approximately an order of magnitude higher for the majority of the domain except in the near vicinity of the thruster exit.

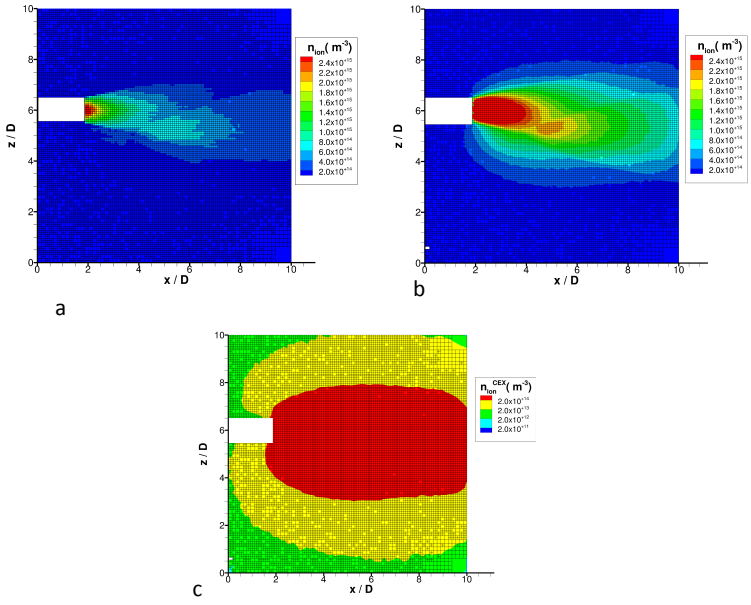

Fig. 1.3 Comparison of ion with an electric field (a) versus ion-no electric field (b) and CEX ion – no electric field (c) number density spatial distributions for the triple thruster simulation in a chamber at y/D=5.

The structure of the ion velocity profile is complex and certainly represents the confluence of a number of factors. If the electric field is artificially turned off, it can be seen in Fig. 4b that the ion spatial distribution is very different from that shown in Fig. 4a and the nature of the expansion in the chamber is changed. The effect is even more pronounced if a similar comparison is made for the CEX ions, as shown in Figs. 3c and 4a. The magnitude of the electric field is insufficient to accelerate the beam ions, however, it has a significant effect on the acceleration of the slower CEX ions. Comparison of Figs. 3c and 4a shows that when the electric field is artificially removed, the CEX ions strongly tend to remain in the interaction region and slow down the total ion (sum of beam and CEX ions) expansion seen in Fig. 3b. The total ion velocity is due to the complex interaction of beam ions, neutrals, and the acceleration provided by the E-field for CEX ions. Given the sensitivity of the results to this acceleration mechanism, the adequacy of the electric potential given by the Boltzmann relationship should be addressed in future.

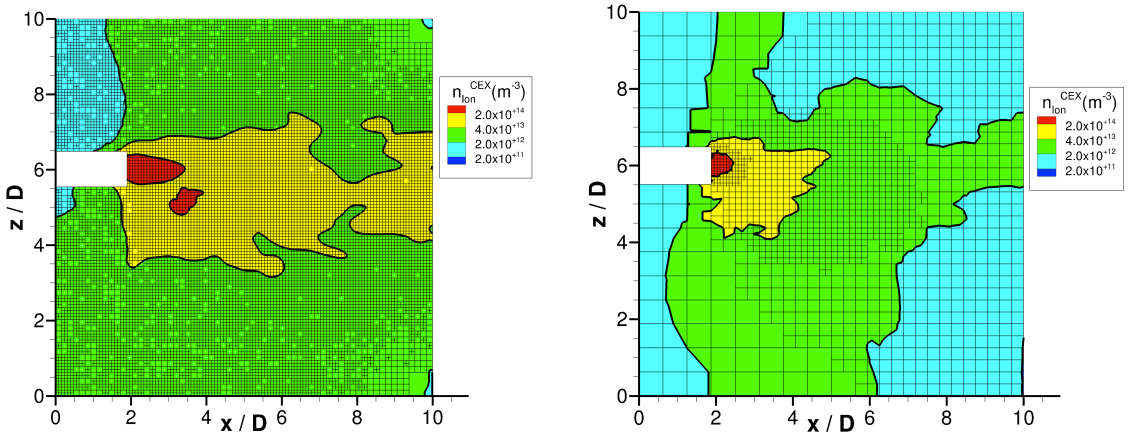

Fig. 1.4 CEX-formed ion number density profiles for triple thruster simulation at y/D = 5 for a

chamber versus space background condition.

2. Rajan group. This component of the project characterized and designed new materials under extreme electric field environments under both vacuum and low gas pressure environments. The overall result from the atom scale characterization component of this project is an experimentally validated description of degradation mechanisms and gas-surface reactions under such extreme conditions. To accomplish this, we developed a new capability to measure in situ gas-solid reactions at the atomic scale, which we linked with density functional theory modeling of field degradation mechanisms under extreme environments and reactive force field (ReaxFF) molecular dynamic modeling of diffusion and interfacial chemistry as a function of environment. This research exploited several areas associated with these accomplishments:

- Atomic scale measurements of in situ gas-solid reactions through the development of the first fully integrated environmental reaction cell with atom probe tomography (APT), while adapting the cell to accommodate a wide range of gases (for example, hydrogen);
- Analysis of the interface resulting from ingress of gaseous species as a function of surface chemistry, gas species, and environmental conditions through the integration of ReaxFF simulations performed at Penn State with APT measurements from University at Buffalo; and
- Identification of degradation mechanisms under extreme environments through DFT calculation of evaporation field and pathways, with APT measurements providing an input and calibration of the DFT calculations.

This work therefore addresses and links three separate length scales: (i) material scale by capturing the reaction between a material and a gaseous or plasma environment as a function of temperature and pressure; (ii) atomic scale by measuring the diffusion and interfacial chemistry resulting from the reaction; and (iii) electronic scale by defining the degradation mechanism as a function of surface chemistry and environmental conditions. Therefore, this project develops an approach for surface design in order to slow degradation under extreme conditions by developing unique capabilities addressing the complex interactions across length-scales.

Further, we quantitatively investigated with APT the effect of temperature on the interfacial transition layer sub-oxide species due to the thermal oxidation of silicon [7], studied the interfacial chemistry under extreme fields [7-10], and calculated the evaporation pathways under extreme electric fields [11-12]. These thrusts lead to defining the relationship between interfacial chemistry with material chemistry and environmental conditions, provided targeted design guidelines for extreme environments, and identified degradation mechanisms of materials under extreme environments through DFT calculation of evaporation fields, providing surface chemistry – evaporation physics relationships. These accomplishments derived from this project are highlighted in the following sections.

In-Situ Atomistic Measurements of Gas-Solid Reactions

We designed and built an integrated environmental cell for APT, and specifically a local electrode atom probe (LEAP), with laser for thermal excitation [8]. With this, we can control the exposure of samples to gases at high temperatures. This also allowed us to study surface reactions without the presence of native oxides or contamination, better simulating the space environment. The reaction chamber is integrated onto the current atom probe system so that gas reactions can occur and be analyzed via atom probe without removing the sample from vacuum. The sample can be heated to temperatures greater than 600 ^{o}C and with fine control of the gas pressure. Gases are inlet into the reaction chamber and the sample can be heated to a desired temperature. While the sample is at a high temperature, a gas is introduced into the chamber and held for some time so that reactions occur between the gas and the material. The material can then be analyzed in the atom probe, in terms of chemistry, atom positions, and bonding. The reaction chamber is integrated into the APT (Figure 2.1), thereby allowing for in-situ measurements. While remaining under high vacuum, the subsequent APT analysis provides detailed information on changes to chemical microstructures following the reactions with near-atomic resolution. . This system with its unique design and capabilities is the first such system in the US.

Building on our initial design, we modified the system to consider a wider range of gaseous environments. For example, hydrogen is weakly interacting, leading to difficulty in imaging with APT. To counter this challenge, the existing environmental chamber was modified to safely introduce gases such as Deuterium (D2) at pressures up to 900 mbarr, with base pressure at 10^{-8} mBarr, while reducing the transfer time from reaction to analysis to minutes instead of hours [13]. We have successfully detected H and D (Figure 2.1), and have repeated the experiment under different surface chemistries, providing a relationship between surface chemistry and the change of chemistry under an extreme environment.

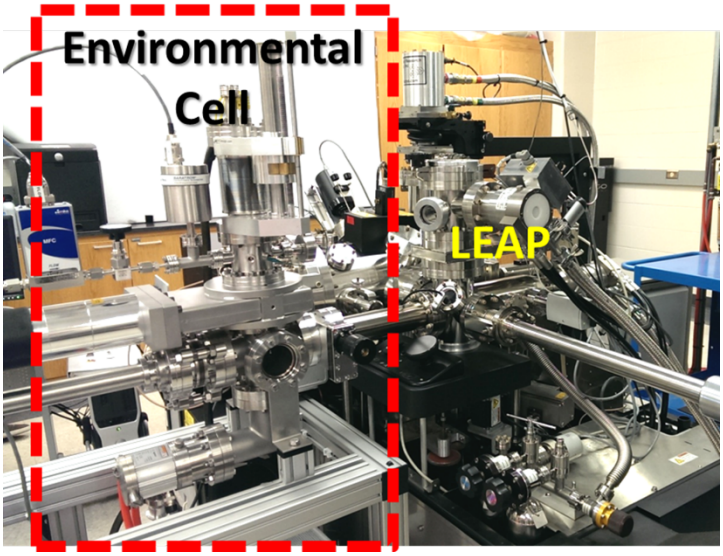

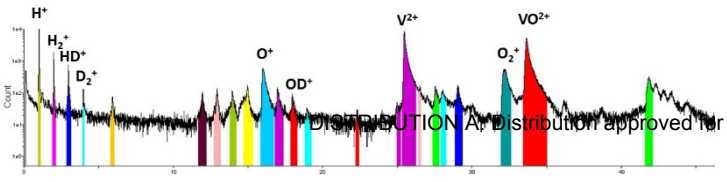

Figure 2.1. (Top) Fully integrated environmental chamber for performing in situ gas-solid or plasma-solid reactions with atomic scale characterization of the surface chemistry. The development and integration of this reaction chamber provides the only current system with its capabilities in the US. (Bottom) Modifications have been made in the final phase of the project to allow us to study

a wider range of gases. For example, we have measured the surface interaction of hydrogen under extreme conditions, allowing us to characterize the role of hydrogen embrittlement. With these modifications, we are capable of studying a wide range of chemical environments applicable for space conditions.

Interfacial Characterization of Gas-Solid Reactions in Extreme Environments

We utilized and advanced an approach for quantitatively characterizing the interfacial region resulting from a gas-solid reaction as a function of temperature. The results were qualitatively compared with ReaxFF simulations to provide a direct comparison between atom probe derived chemical profiles and atomistic-scale simulations of transitional interfacial layers [7]. Beyond providing comparison, the linkage of these two approaches provide a more complete description of the diffusion process. ReaxFF modeling describe hyper thermal oxidation, are dynamic, are at a smaller time scale and detect monolayers. Meanwhile, APT described plasma oxidation, are static, cover a longer time scale, and detect at the sub-nano scale. Therefore, this work beyond providing experimental component to the simulations and providing physical description to the experiments also provides a wider range of reaction types and spans length- and time-scales beyond what was previously possible. This work demonstrates the first direct comparison between atom probe derived chemical profiles with atomistic-scale simulations to study the oxidation mechanism of silicon. From a methodology perspective, the qualitative agreement between experiment and simulation lays the foundation for using this approach to interpret fundamental mechanisms of materials behavior.

The APT results for gas-solid reaction at different temperatures is shown in Figure 2.2. Each sphere in these images is an experimentally measured atom, with respective color code corresponding to chemistry of the atom. The diffusion of oxygen into silicon is clearly seen at both temperatures, with the diffusion greater at higher temperature than at lower temperature. Further thorough analysis of the interfaces was done through proximity histograms across the silicon and silicon oxide interface for both temperatures. A region of inter-diffusion and two distinct regions consisting of bulk silicon (region I) and an oxide phase (region III) can be clearly seen at both temperatures.

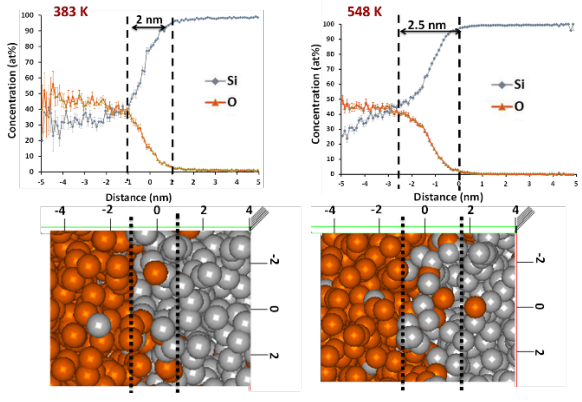

Figure 2.2. APT measurement of gas-solid reactions as a function of temperature. (Top) The interfacial thickness is measured, with an increased thickness found with increasing temperature. Comparison of this experimental result with ReaxFF simulations provides a description of the diffusion mechanism. (Bottom) Atomistic scale image of diffusion and chemical ingress, with each

orange sphere representing an experimentally measured oxygen atom and each gray sphere representing an experimentally measured silicon atom.

Comparison with ReaxFF results provided validation of the APT characterization, while also providing description of the diffusion mechanism. At low gas concentration, Si^{4+} is greater at low temperature than at high temperature, indicating that the initial growth of SiO_2 layer is faster at low temperatures; however, as gas concentration increases, the silica layer grows faster at higher temperatures but with nucleation starting later. Also, the number of sub-oxide species increases with increasing temperature. We can therefore experimentally measure the four stages of growth at low temperatures (Figure 2.3): growth of sub-oxides and an incipient silica layer growth; continued growth of sub-oxides with inward growth rate of sub-oxides dropping due to high activation energy; and growth of sub oxides and silica then slows down. In addition to providing a direct comparison between different physics descriptions, this work also has implications for the analysis of bonding information in bulk versus interfacial regions in APT coupled to bond length and bond angle information in ReaxFF.

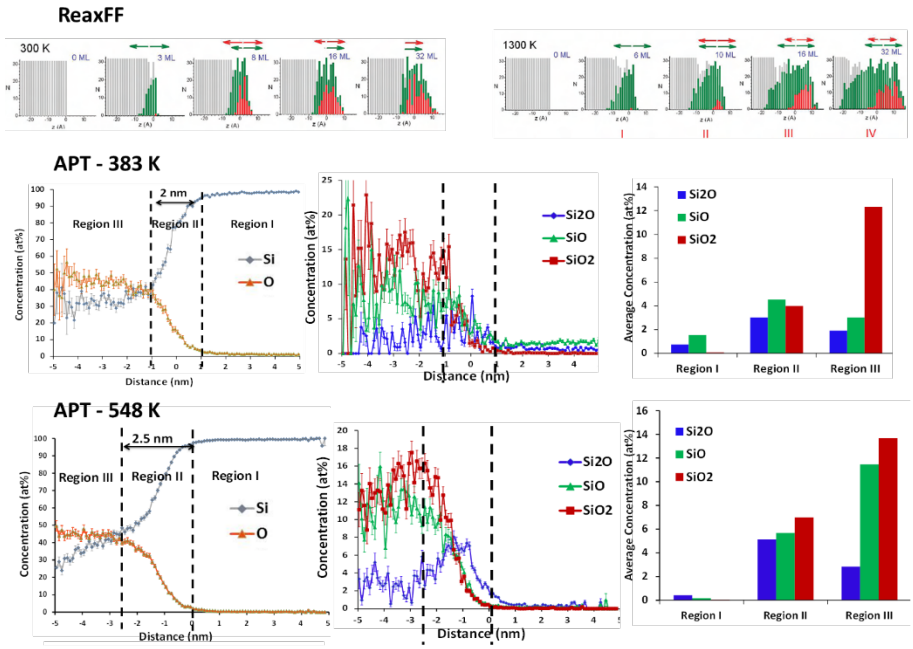

Figure 2.3. Comparison of ReaxFF simulations with APT measurements for diffusion as a function of temperature. From this, we are able to describe the oxide growth mechanism. For example, at higher temperature, we find increased growth of suboxides with time as the activation energy barrier is surmounted at higher temperatures. APT and ReaxFF provide information spanning a wider range of length and time scales, as well as providing different descriptions of the diffusion process (static versus dynamic). These results are in agreement with each other and therefore we have a more complete understanding of the growth mechanism as a function of environmental conditions than was previously available.

Identifying Degradation Mechanisms Under Extreme Conditions

The degradation mechanism of metallic surfaces under extreme conditions were modeled via density functional theory (DFT) with the inputs calibrated via APT experiments [11,12]. From this study, we are able to understand the effects of extreme electrical fields on the charge distribution of metallic surfaces and bond character at the moment of evaporation (ie. degradation), while also linking surface structure and neighborhood chemistry with field evaporation pathways. We modeled the surface bonding and charge distribution and then correlated the DFT results with experimental measurements by comparing the calculated evaporation fields with atom probe tomography measurements. The evaporation fields of different surface neighborhood chemistries were calculated. Based on either the shared charge density between surface atoms or charge localization around an atom, we are able to describe the process for breaking surface bonds and understand the relationship between surface chemistry and degradation. This combined APT-DFT work provides a definition of the surface chemistry-degradation relationships, which can be used to rapidly screen different surface chemistries to identify the best chemical surface design to limit the degradation rate in space environments.

We computationally characterized the field evaporation process by modeling the charge density at the surface of the material as a function of electric field, thereby identifying the charge distribution and directionality just prior to field evaporation. Further, the electron localization function just prior to evaporation was analyzed in order to characterize the bond breaking process between the evaporating ions and the surface. The effects of the electric field on our test system ($L1_2$-Al_3Sc) is shown in shown in Figure 2.4, with a comparison made between experimental APT results and the DFT calculations. We observe a significant modification of the charge distribution that surrounds the ion when the evaporation field is incorporated. The colors of the charge density correspond to: red with a positive charge per volume and blue with a negative charge per volume.
Beyond defining the critical bonding changes with increasing electric field, we also identify the difference in mechanism for evaporation. For Al-Al dimer on the surface, the primary charge is between the surface and the dimer, with the distribution shared for the dimer. This shared charge explains why Al-Al more easily evaporates in this configuration as a dimer instead of as single ions. Conversely, Al-Sc dimer on the surface has a significant charge in between the Al and Sc atoms, and also isolated charges between the atoms and the surface. This configuration of the charge density describes the mechanism for the atoms evaporating as separate ions. Therefore, by calculating the charge density, we have been able to differentiate two separate evaporation mechanisms under changing electric field.

To represent the atom probe data, we develop an ‘ion evaporation map’. In the case of multi-hit events (that is, more than one ion detected at the same time), the ion evaporation map can be used to plot the pair-wise interactions. The axes of an ion evaporation map are mass-to-charge (m/n) 1 and m/n 2, where each axis represents one of the ions in a multi-hit event. The inverted ion order is also included, so that the m/n 1 = m/n 2 line is a line of symmetry. A majority of the multi-hit events are not due to dimer evaporations, but we address this noise issue by considering only relative differences in the multi-ion events. The ion evaporation map is then correlated with relative bond strengths under extreme field, where the greater the likelihood of dimer evaporations indicating an

increased bond strength. That is, it is more favorable to break all the surface bonds than to break the single bond between the dimer ions. This is clearly demonstrated in Figure 4, with the charge build-up with the surface bonds for Al-Al case, and build-up between the Al and Sc atoms in the Al-Sc case. This figure therefore correlates the evaporation mechanism with the experimental data, providing a level of physics not provided by the experimental data alone [14-18]. This approach, which is extendable to any metallic chemistry and structure, as well as extendable to ceramic systems, defines the role of electronic evaporation.

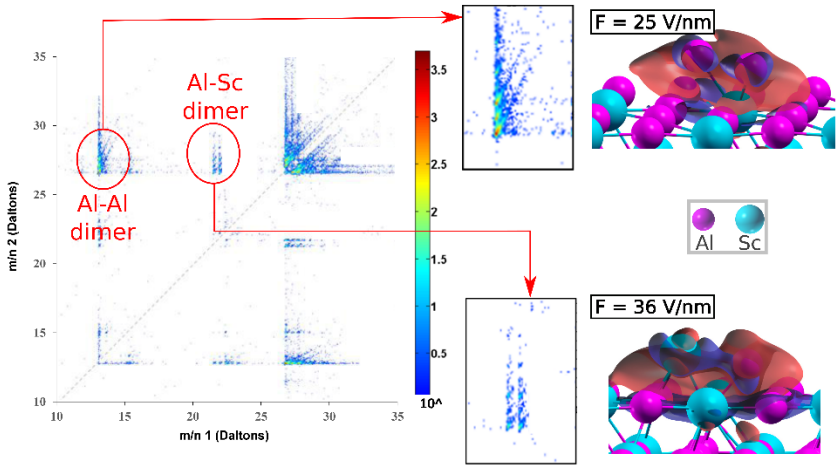

Figure 2.4. Definition of the degradation mechanism under extreme electric fields, by comparing experimental APT data with charge density distributions. The inset regions focus on different surface chemistries, with the overall chemistry of the material for these two regions being nearly equivalent. The number of Al-Al dimers is seen to be significantly higher. The DFT results describe the reason for this being the charge localization (shown as dark blue) around the Sc atom, resulting in Sc evaporating as a single ion. This work shows how we are able to screen the surface chemistry design space to identify chemistries which most inhibit material degradation under specific environmental conditions.

3. van Duin group. During the first years of this project we have demonstrated the viability of the ReaxFF reactive force field method for studying the response of realistic, complex materials and material interfaces to the extreme space environment. The ReaxFF capability was established for various polymers (Kapton, Teflon [19]), ceramics (silica[7], silicon) metals (aluminium[20,21]) and graphite[22] – while a range of colliding species were employed, ranging from noble gas cations to water, oxygen atoms[19], water clusters [25], silica and metal oxide nanoparticles[22]. We demonstrated that ReaxFF can be trained to reproduce Density Functional Theory (DFT) data for noble gas cation repulsive interactions with organic and inorganic materials providing a highly transferable simulation tool that can address multi-material interfaces inaccessible to simpler empirical force fields. We have been using this improved ReaxFF description to study high-velocity Argon collisions with carbon, silicon and aluminium surfaces. Furthermore, in collaboration with the Levin group, we have studied the effects of water-cluster collisions on silica oxide and silica suboxide surfaces[23-26] (Figure 3.1). From this work we obtained a detauled, atomistic-scale view of how the properties of the

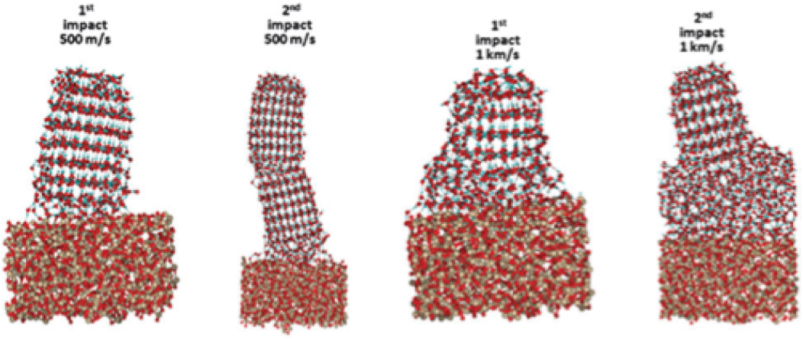

Figure 3.1: Side view of first and second impacts of crystal ice clusters on a suboxide silica surface at 500 m s^{-1} and 1 km s^{-1} impact velocities.

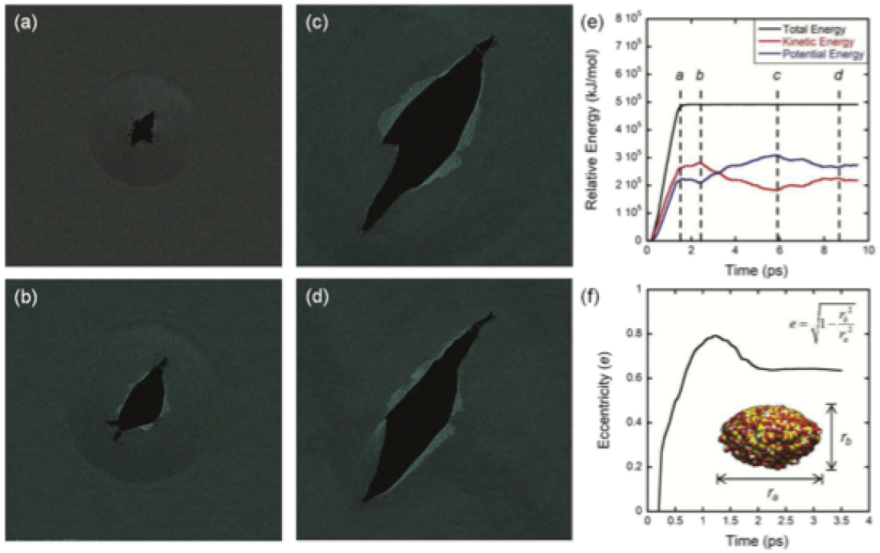

Figure 3.2: Evolution of the atomistic structures and energy during the penetration of pristine graphene by the nickel projectile: (a)-(c) Atomistic structures of graphene taken at times a-c, indicated in (e); (d) Most frequently found bonds between nickel and carbon atoms; (e) Energy evolution of graphene during the penetration; (f) Structure evolution of the nickel projectile: deformation of the projectile is expressed by using the concept of eccentricity. The inset shows the nickel projectile at maximum deformation.

silica surface - including surface chemistry, thermal conductivity and water-accumulation and removal during collisions with high-velocity water and ice clusters.

The ReaxFF results were validated against experimental data. In particular, we obtained one-to-one comparisons between ReaxFF and Atom Probe Tomography (Rajan group) results for oxygen diffusion in silicon. Furthermore, we compared ReaxFF Kapton and Teflon response to high-velocity oxygen collision to atomic oxygen erosion yield data from the MISSE 2 experiments[19] and found excellent qualitative and good quantitative agreement. Finally, we established the ReaxFF capability for complex, multi-material, high velocity collision simulations by reproducing published experimental trends from Li et al. (Science 2014, **346**, 6213) for silica and collision with graphene surfaces[22] (Figure 3.2).

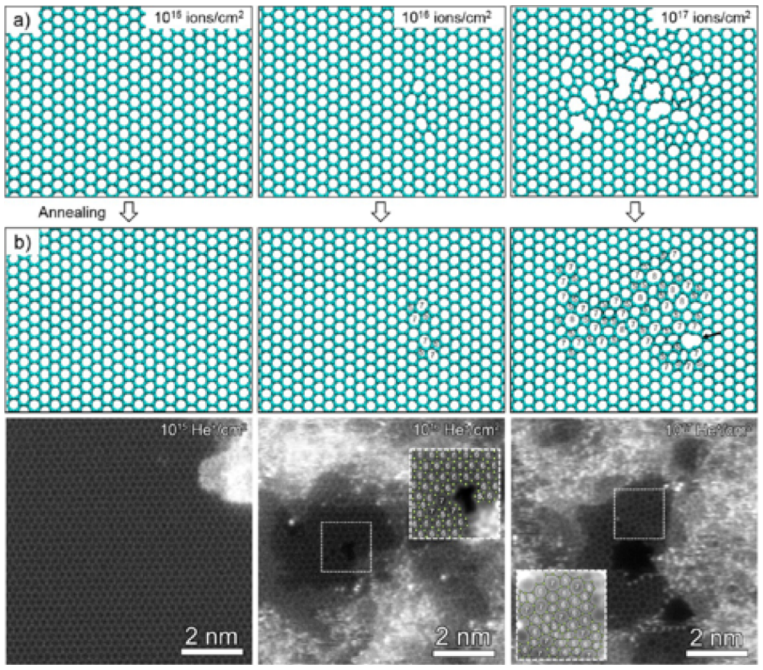

Figure 3.3: Comparison of pre-annealed (a), post-annealed (b) ReaxFF graphene structures after exposure to noble-gas cations and comparison with experimental STEM results (bottom).

In order to connect to the noble-gas collision experiments in the Sedwick-group, we extended the ReaxFF noble-gas/carbon description to the highly repulsive 'inner wall' distances (sub-Angstrom). Typically, ReaxFF underestimates the repulsive atom-atom interactions at that distance, which limits its applicability to high-velocity (keV kinetic energies) impacts. We added a strongly repulsive exponential function - which fades quickly for distances beyond 1 Å, so that it does not affect ReaxFF equilibrium structures and transition states - and fitted this function to a mixture of DFT calculations (0.5-1 Å) and ZBL-potential data (<0.5 Å). In order to validate this ReaxFF extensin, we collaborated with a team from Lockheed Martin and Oak Ridge National Lab to compare ReaxFF graphene damage structures as a function of noble gas exposure to experimental results. We found excellent agreement between ReaxFF post-annealing damage statistics and experimental scanning transmission electron microscopy (STEM) images (Figure 3.3) [27].

In addition to this work, we collaborated with various groups on the development and validation of ReaxFF parameters for various spacecraft-relevant materials [27-34] (aluminium- including oxidation and H-embrittlement, ZBr, silicene, Si/Ge, graphene, B/N doped carbon) and on metadynamics and hybrid Monte Carlo/Molecular Dynamics ReaxFF options (Figure 3.4) [35-36] - which greatly enhance the ReaxFF-accessible time scales, as such enabling ReaxFF based simulations that are far closer to experimental conditions.

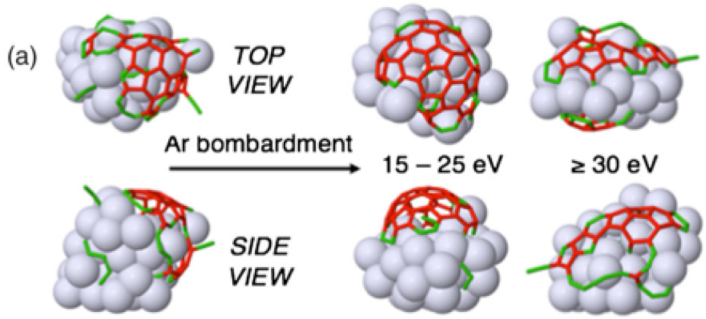

Figure 3.4: Structures obtained from ReaxFF hybrid Grand Canonical Monte Carlo/MD simulations of carbon growth on a Ni-nanoparticle during bombardment with Ar-cations.

These results indicated that the ReaxFF reactive force field method is highly suitable for establishing the response of materials and material interfaces to spacecraft environments. All simulations were performed at a reasonable computational expense – using 20 processors or less, with simulation times ranging from a couple of hours to – at most – a week. As such, these results indicate that the ReaxFF method shows great promise as a computational tool for designing the next generation of spacecraft materials.

4. Sedwick group. Throughout the duration of this AFOSR grant, the Space Power and Propulsion Lab (SPPL) has been focused on supporting the various analytical efforts through experimental contributions [37] as well as independently researching the effects of formation flight electrostatic thruster plumes on spacecraft materials [38]. Experimental collaborations were performed with both the Levin and Rajan groups which both involved the use of ion plumes from an electrostatic source.

The experimental effort with the Levin group focused mainly on the analysis of the charge-exchange (CEX) environment of the plasma plume from a lab-grade ion engine, the SPPL-1 Ion Source. The analysis involved using a Retarding Potential Analyzer (RPA) to measure the primary energy distribution of the plume at axial distances of 2-8 centimeters along the plume centerline (Figure 4.1). The primary goal of this analysis was to determine the evolution of the CEX environment as it progressed from the thrust exit as well as to possibly determine the chamber effects on said environment. The main role of the experimental efforts here were to scan the plasma environment and use these measurements as a basis for a CEX simulation using a Monte Carlo method to examine potential effects on micro-satellites [37].

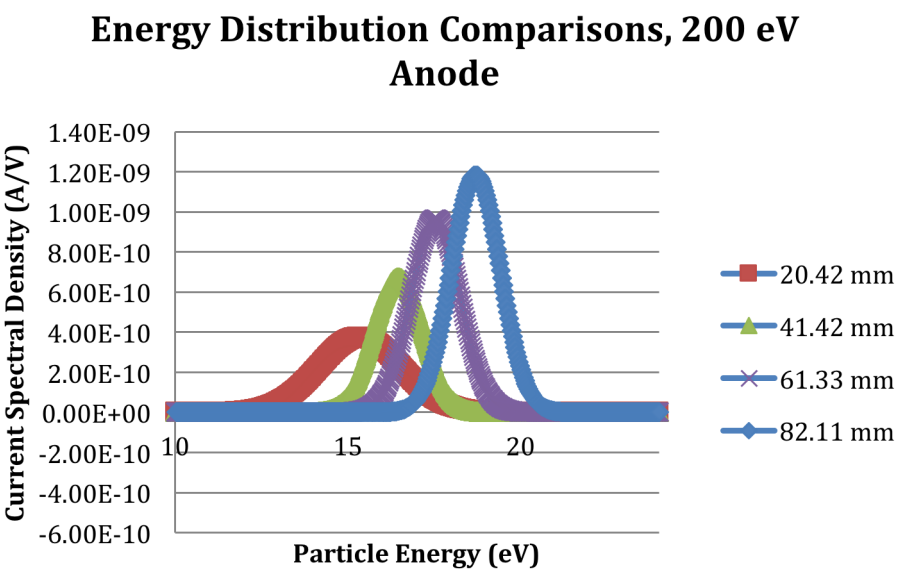

Fig. 4.1: CEX energy distributions

The experimental efforts with the Rajan group focused on implanting silicon microtips with argon ions at varying energy levels to look at possible penetration depths and potential sputtering of the microtips through the use of an atom probe tomographer [38] (APT). This device would be able to destructively analyze the microtips and be able to look at structural defects down to the crystalline level. As a result of ion bombardment at 250 eV with argon, argon atoms were detected within the microtips at varying densities due to the difference in

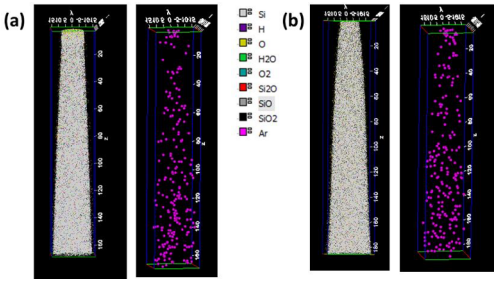

Fig. 4.2: APT images of (a) 50 and (b) 150 Ar monolayer bombarded samples of silicon [2]

exposure times (Figure 4.2).

Mathematical Modelling and Analysis of Sputter

In order to understand the experimental results, the SPPL group developed an internal mathematical model based on the material parameters of the sputter target. Using the Eckstein [39] method of calculating sputter yield as a basis, the group has been able to model the sputter depth of certain argon and xenon sputter reactions based on the incident ion rate (F), crystalline lattice parameter (d_{layer}), and mass density [40]. From these parameters, the quantities of number of atoms per layer, sputtered atoms, number of layers sputtered, and ultimately sputter depth can be found. Equations (1-5) make up the basis of this model are displayed above.

$$Y(E_0) = qs_n^{KrC}(\varepsilon)\frac{\left(\frac{E_0}{E_{th}} - 1\right)^{\mu}}{\frac{\lambda}{W(\varepsilon)} + \left(\frac{E_0}{E_{th}} - 1\right)^{\mu}}$$

$$SA = Y(E_0)Ft$$

$$APL = \frac{\rho_{Al} d_{layer} EA}{m_{Al}}$$

$$LS = {}^{SA}/_{APL}$$

$$SD = LS * l_{lattice}$$

Equation 1-5: Sputter Model Equations [4]

Sputter Yield Data Collection

The main effort of the SPPL group focused on observing the effects of xenon ion plume impingement on spacecraft materials in order to analyze the potential damage exposure of formation flight spacecraft to these beams. Not only is the primary spacecraft structure in danger from erosion, the anti-reflective (AR) coating of solar cell coverglass is also highly at risk. It has been noted that if the AR coating is eroded away, the efficiency of the solar cell will fall by 2.6% [41]. The main damage mechanism for these materials is sputtering, the removal of surface atoms through the use of energetic particles, via xenon beam. To assess the damage potential of the beam, the sputtering yield of each reaction must be determined.

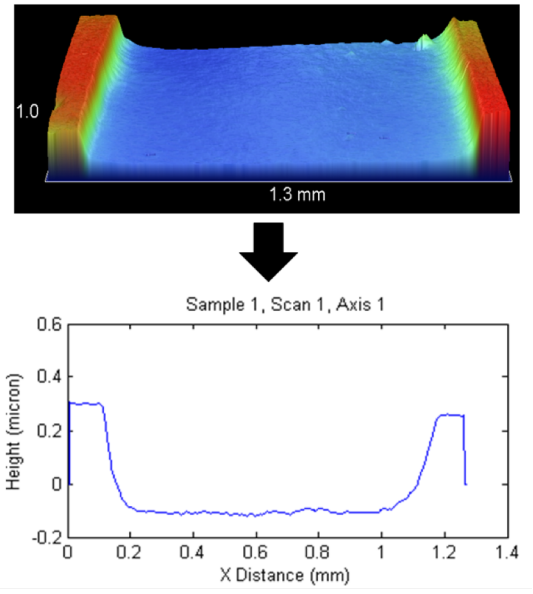

Fig. 4.3: Aluminum 1500 eV erosion Profile

The main materials observed in this effort are aluminum, magnesium fluoride (MgF_2) and indium tin oxide (ITO). These materials have varying degrees of sputter yield data associated with them. The sputter interaction with the most data is the Xe→Al sputter reaction collected in two different efforts from Rosenberg [42] and Tartz [43] with a 50 year gap in between. Similarly, there has been an effort to characterize the

sputter yield of MgF_2 at low energies (<400 eV) by Yalin [39] and some experimental observations of ITO by Hu [44]. These materials are coated onto silicon wafers in the thickness of 500 nm (MgF_2 and ITO) and 1000 nm (Al). The silicon wafer base allows for a comparatively flat surface to coat the materials on as well as to provide a strong base for examination via profilometer.

There are many such examples of experimental efforts looking at the effects of ion plumes interacting with the spacecraft of the plume's origin on its varying components, such as the ion optics grids [45] or solar panels [46,47]. However, very few efforts have looked at the effect of the ion plume at standard operating energies on other spacecraft beyond computational simulation [48].

Through an internally developed sputter model and the use of an optical profilometer, the erosion depths of each material sample can be determined and then used to assess the sputtering yield for a set of testing conditions. The energy ranges of the experiment vary from between 500-1500 eV in 250 eV increments for the MgF_2 and the ITO testing and from 1200-1600 eV for aluminum testing. A sample of the profile data

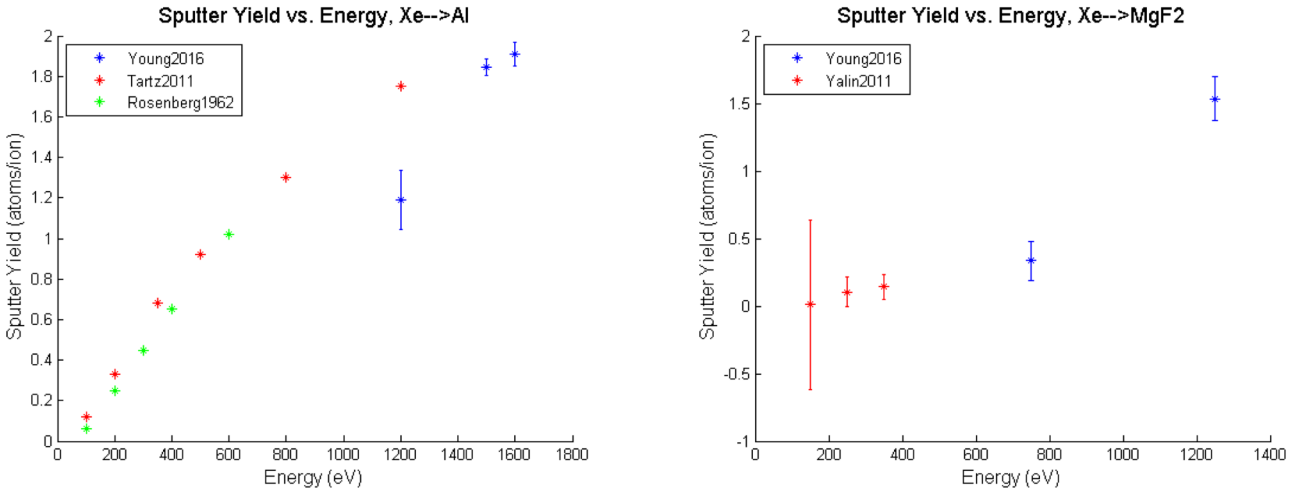

Fig. 4.4: Experimental Sputter Yields for Al (left) and MgF_2 (right)

generates is depicted in Figure 4.3.

Results from the experiments (Figures 4.4 and 4.5) show that the majority of the sputter yields fit with the expected logarithmic trends. Results from the aluminum testing show that the SPPL data is mostly in line with the Tartz data based on the trend of the data. The 1200 eV data point shows approximately 30% disagreement with the previously published data. However, the reported data from this effort is higher than the Eckstein approximation of the sputter yield based on previous experimental data. Sputter data for the AR coatings also seem to follow

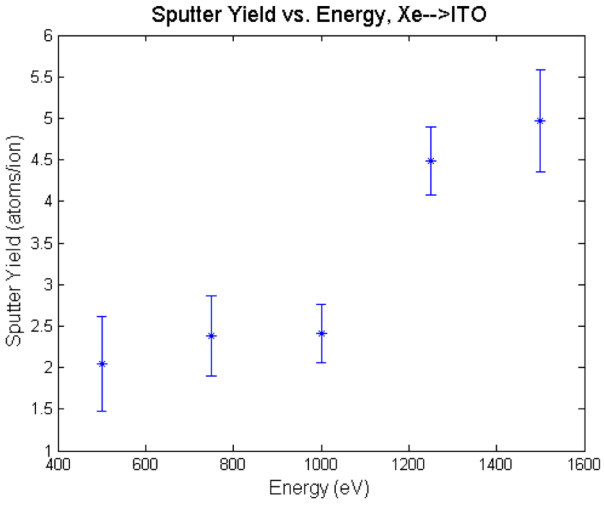

Fig. 4.5: Experimental Sputter Yields for ITO

expected trends, although there is a much larger jump in yield than expected for ITO between 1000 and 1250 eV. From the sputter data above, it can be inferred that ITO, while space-rated for solar cell coverglass, would erode very quickly under the influence of an ion plume, even in the energy regime of a Hall thruster [44]. MgF_2, which has very similar anti-reflective properties, has a much lower sputter yield and therefore has a much higher resilience to ion thruster bombardment. Complete sputter data for all materials are shown in Tables 4.1-4.3.

Also, there are also possible point defects that have a much higher sputter depth than the majority of the exposed sample area. This has been shown, as in Figure 4.5, by the existence of craters which extend past the coated material to the silicon foundation. It can be inferred that, although the collective erosion depth can be used to estimate the sputter yield, there will be point defects along the surface that cannot be accounted for in the sputter model. These "craters" can possibly be explained by non-uniform surface topography that are not normal in incidence to the beam, which will only increase the sputter yield [39,40,49,50] or localized melting.

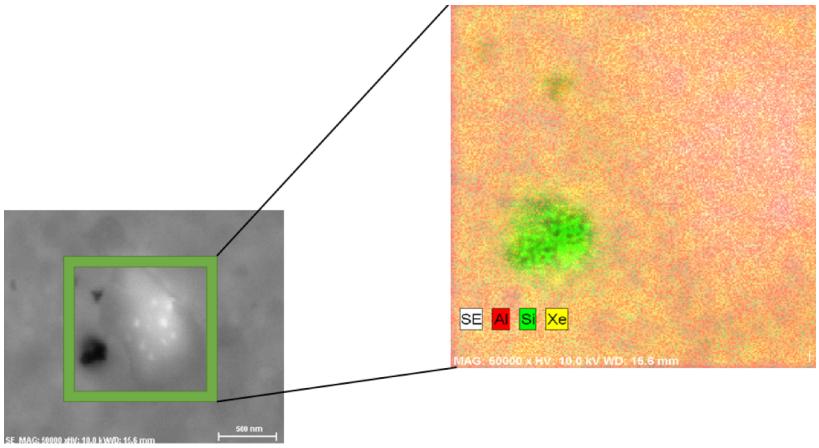

Fig. 4.4: Close-up of EDS scan of Al sample sputtered by 1500 eV Xenon beam [13]

Table 4.1: Al Sputter Data

Energy (eV)	Sample Number	Average Ion Rate (ions/sec)	Atoms Lost (atoms)	Sputter Yield (atoms/ion)	Average Sputter Yield (atoms/ion)
1200	1	5.80E+13	2.90E+16	1.391	1.1891
1200	2	4.91E+13	3.18E+16	1.079	
1200	3	4.72E+13	3.11E+16	1.097	
1500	1	3.94E+13	4.28E+16	1.812	1.8437
1500	2	1.59E+13	1.84E+16	1.929	
1500	3	2.55E+13	2.74E+16	1.790	
1600	1	3.14E+13	3.77E+16	2.003	1.9107
1600	2	3.67E+13	3.42E+16	1.940	
1600	3	4.18E+13	3.59E+16	1.789	

Table 4.2: MgF_2 Sputter Data

Energy (eV)	Sample Number	Average Ion Rate (ions/sec)	Atoms Lost (atoms)	Sputter Yield (atoms/ion)	Average Sputter Yield (atoms/ion)
750	1	2.94E+13	1.70E+16	0.321	0.3349
750	2	2.97E+13	1.76E+16	0.330	
750	3	2.25E+13	1.13E+16	0.280	
750	4	1.19E+13	8.78E+15	0.410	
1250	1	3.61E+13	1.20E+17	1.854	1.5334
1250	2	2.85E+13	7.01E+16	1.367	
1250	3	2.69E+13	8.23E+16	1.700	

Table 4.3: ITO Sputter Data

Energy (eV)	Sample Number	Average Ion Rate (ions/sec)	Atoms Lost (atoms)	Sputter Yield (atoms/ion)	Average Sputter Yield (atoms/ion)
500	1	5.66E+12	9.22E+15	2.714	2.04
500	2	6.26E+12	6.22E+15	1.657	
500	3	5.70E+12	5.99E+15	1.751	
750	1	5.37E+12	9.72E+15	3.018	2.38
750	2	1.02E+13	1.32E+16	2.162	
750	3	9.89E+12	1.57E+16	2.639	
750	4	1.44E+13	1.47E+16	1.699	
1000	1	1.37E+13	1.13E+16	2.754	2.4112
1000	2	1.11E+13	9.29E+15	2.789	
1000	3	1.48E+13	9.72E+15	2.188	
1000	4	1.73E+13	9.93E+15	1.914	
1250	1	1.15E+13	9.31E+15	5.396	4.4841
1250	2	1.25E+13	9.47E+15	5.051	
1250	3	1.38E+13	8.49E+15	4.102	
1250	4	2.43E+13	1.48E+16	3.387	
1500	1	1.38E+13	1.32E+16	6.353	4.9737
1500	2	1.50E+13	8.42E+15	3.741	
1500	3	1.28E+13	1.20E+16	6.228	
1500	4	1.54E+13	9.90E+15	3.572	

References

1. Hyakutake, T. , Nishida, M., Kuninaka, H. and Toki, K., "DSMC-PIC Analysis of a Plume from MUSES-C Ion Engines," *Transaction of the Japan Society for Aeronautical and Space Sciences*, Vol. 46, 2003, pp. 24-30.
2. Wang, J. , Cao, Y., Kafafy, R., Pierru, J. and Decyk, V., "Simulations of Ion Thruster Plume-Spacecraft Interactions on Parallel Supercomputer," *IEEE Transactions on Plasma Science,* Vol. 34, No. 5, 2006, pp. 2148-2158.
3. Korkut, B., Levin, D. and Li, Z., "Three Dimensional Simulation of Ion Thruster Plumes using Octree Adaptive Mesh Refinement," *IEEE Transactions on Plasma Science*, Vol. 43, No. 5, May, 2015,
4. Korkut, B. and Levin, D., "Three Dimensional Simulations of Backflows from Ion Thruster Plumes using SUGAR," *Accepted to Journal of Propulsion and Power, July 2016.*
5. B. Korkut, "Development of a Scalable Gas-Dynamic Solver with Adaptive Mesh Refinement," Ph.D thesis, The Pennsylvania State University, Aug. 2015.
6. M. S. Ivanov, A. V. Kashkovsky, S. F. Gimelshein, G. N. Markelov, A. A. Alexeenko, Ye. A. Bondar, G. A. Zhukova, S. B. Nikiforov and, P. V. Vashenkov, "SMILE System for 2D/3D DSMC computations," *Proceedings of the 25th International Symposium on Rarefied Gas Dynamics*, Publishing House of the Siberian Branch of the Russian Academy of Sciences, 2007, M. S. Ivanov and A. K. Rebrov, Novosibirsk, pp. 539-544.
7. S. Dumpala, S.R. Broderick, U. Khalilov, E.C. Neyts, A.C.T. van Duin, J Provine, R.T. Howe, K. Rajan. "Integrated atomistic chemical imaging and reactive force field molecular dynamic simulations on silicon oxidation." *Applied Physics Letters* 106, 011602 (2015)
8. S. Dumpala, S.R. Broderick, P.A.J. Bagot, K. Rajan. "An integrated high temperature environmental cell for atom probe tomography studies of gas-surface reactions: instrumentation and results." *Ultramicroscopy* 141, 16-21 (2014)
9. S. Srinivasan, K. Kaluskar, S. Broderick, K. Rajan. "Extracting features buried within high density atom probe point cloud data through simplicial homology." *Ultramicroscopy* 159, 374-380 (2015)
10. S. Broderick, J. Peralta, S. Samudrala, K. Kaluskar, B. Ganapathysubramanian, K. Rajan. "Application of computational homology and graph-theoretic approaches for quantitative chemical imaging in atom probe tomography." *Microscopy and Microanalysis* 19, S2 930-931 (2013)
11. C. Loyola, J. Peralta, S.R. Broderick, K. Rajan. "Impact of extreme electrical fields on charge density distributions in alloys." *Journal of Vacuum Science and Technology*, Under Review
12. J. Peralta, S.R. Broderick, K. Rajan. "Mapping energetics of atom probe evaporation events through first principles calculations." *Ultramicroscopy* 132, 143-151 (2013)

13. S. Dumpala, D. Haley, S.R. Broderick, P.A.J. Bagot, M.P. Moody, K. Rajan. "In-situ deuterium charging for direct detection of hydrogen in vanadium by atom probe tomography." *Microscopy and Microanalysis* 21, S3 695-696 (2015)
14. F. Vurpillot, W. Lefebvre, J.M. Cairney, C. Oberdorfer, B.P. Geiser, K. Rajan. "Advanced volume reconstruction and data mining methods in atom probe tomography." *MRS Bulletin* 41, 46-52 (2016)

15. S. Broderick, K. Rajan. "Extracting chemistry-property relationships by mining atom probe evaporation events." *Microscopy and Microanalysis* 22, S3 700-701 (2016)
16. .M. Cairney, K. Rajan, D. Haley, B. Gault, P.A.J. Bagot, P-P. Choi, P.J. Felfer, S.P. Ringer, R.K.W. Marceau, M.P. Moody. "Mining information from atom probe data." *Ultramicroscopy* 159, 324-337 (2015)
17. S.R. Broderick, S. Dumpala, S. Padalkar, K. Rajan. "Data intensive imaging for 3D atom probe." *Microscopy and Microanalysis* 20, S3 812-813 (2014)
18. S.R. Broderick, A. Bryden, S.K. Suram, K. Rajan. "Data mining for isotope discrimination in atom probe tomography." *Ultramicroscopy* 132, 121-128 (2013)
19. Rahnamoun, A.; van Duin, A. C. T. *Journal of Physical Chemistry A* **2014**, *118*, 2780.
20. Hong, S. and van Duin, A. C. T., 2015. Molecular Dynamics Simulations of the Oxidation of Aluminum Nanoparticles using the ReaxFF Reactive Force Field. *Journal of Physical Chemistry C* **119**, 17876-17886.
21. Verners, O., Psofogiannakis, G., and van Duin, A., 2015. Comparative molecular dynamics study of fcc-Al hydrogen embrittlement *Corrosion Science* **98**, 40-49.
22. Yoon, K., Ostadhossein, A., and van Duin, A. C. T., 2016. Atomistic-scale simulations of the chemomechanical behavior of graphene under nanoprojectile impact. *Carbon* **99**, 58-64.
23. Li, Z.; Borner, A.; Rahnamoun, A.; Levin, D.; van Duin, A. C. T. "BGK and MD Simulations of H_2O Supersonic Condensed Jets"; AIAA 2014, 2014, Atlanta.
24. Rahnamoun, A. and van Duin, A. C. T., 2015. Study of thermal conductivity of ice clusters after attachment to the silica surfaces using the ReaxFF reactive force field. *Phys. Chem. Chem. Phys.* **18**, 1587-1594.
25. Rahnamoun, A. and van Duin, A. C. T., 2016. Study of Ice Cluster-Amorphous Silica Collision in the Extreme Space Environment using the ReaxFF reactive force field molecular dynamics simulation method. *Journal of Applied Physics* **119**, 095901.
26. Yoon, K., Rahnamoun, A., Swett, J., Iberi, V., Cullen, I. V., Vlassiouk, I. V., Belianinov, A., Sang, X., Ovchinnikova, O. S., Rondinone, A. J., Unocic, R. R., and van Duin, A. C. T., 2016. Atomistic-scale simulations of the defect formation in graphene under noble gas irradiation. *ACS Nano* **published online**.
27. Hong, S. and van Duin, A. C. T., 2016. Atomistic-Scale Analysis of Carbon Coating and Its Effect on the Oxidation of Aluminum Nanoparticles by ReaxFF-Molecular Dynamics Simulations. *Journal of Physical Chemistry C* **120**, 9464-9474.

28. Verners, O., Psofogiannakis, G., and van Duin, A., 2015. Comparative molecular dynamics study of fcc-Al hydrogen embrittlement *Corrosion Science* **98**, 40-49.
29. Psofogiannakis, G. and van Duin, A. C. T., 2015. ReaxFF Simulations of Hydrogen Atom Bombardment of Si,Ge, and SiGe alloy surfaces. *Surface Science* **646**, 253-260.
30. Hong, S. and van Duin, A. C. T., 2015. Molecular Dynamics Simulations of the Oxidation of Aluminum Nanoparticles using the ReaxFF Reactive Force Field. *Journal of Physical Chemistry C* **119**, 17876-17886.
31. Paupitz, R., Junkermeier, C. E., van Duin, A. C. T., and Branicio, P., 2014. Fullerenes generated from porous structures. *Phys. Chem. Chem. Phys.* **16**, 25515-25522.
32. Botari, T., Perim, E., Autreto, P. A. S., van Duin, A. C. T., Paupitz, R., and Galvao, D., 2014. Mechanical Properties and Fracture Dynamics of Silicene Membranes. *Phys. Chem. Chem. Phys.* **16**, 19417-19423.
33. Berdiyorov, G. R., Neek-Amal, M., Peeters, F. M., and van Duin, A. C. T., 2014. Stabilized nanosilicene within bilayer graphene. *Physical Review B* **89**, 024107.
34. Gouissem, A., van Duin, A. C. T., and Sharma, P., 2013. A Reactive Force Field for Zirconium and Hafnium di-Boride. *Computational Materials Science* **70**, 171-177.
35. Neyts, E. C., Ostrikov, K., Han, Z. J., Kumar, S., van Duin, A. C. T., and Bogaerts, A., 2013. Defect healing and enhanced nucleation of carbon nanotubes by low-energy ion bombardment. *Physical Review Letters* **110**, 065501.
36. Joshi, K., Raman, S., and van Duin, A., 2013. Connectivity-Based Parallel Replica Dynamics for Chemically Reactive Systems: From Femtoseconds to Microseconds. *Journal of Physical Chemistry Letters* **4**, 3792-3797.
37. Korkut, B., Levin, D., Young, J., Sedwick, R., Comparison of Ion Thruster Plumes Generated in the SPPL-1 Facility with DSMC Simulations using AMR, 52nd Aerospace Sciences Meeting, AIAA SciTech 2014, AIAA-2014-0139, 13-17 January 2014, National Harbor, MD
38. Young, J., Sedwick, R., Dumpala, S., Rajan, K., High Energy Plume Impingement on Spacecraft Systems, 52nd Aerospace Sciences Meeting, *AIAA SciTech 2014, AIAA-2014-1032, 13-17 January 2014, National Harbor, MD*
39. Behrish, R. and Eckstein, W., *Sputtering by Particle Bombardment*, Springer, 2007
40. Young, J., "Ion Plume Damage in Formation Flight Regimes," Doctoral Yalin, A., et al., "Effect of Ion Sputtering on Transmission of Coverglass with Magnesium Fluoride Coating," 32nd International Electric Propulsion Conference, September 11-15, 2011, Wiesbaden, Germany, IEPC-2011-066
41. Rosenberg, D. and Weiner, K., "Sputtering Yields for Low Energy He^+, Kr^+, and Xe^+ Ion Bombardment," *Journal of Applied Physics*, Vol. 33, No. 5, May 1962, pp. 1842-1845
42. Tartz, M., et al., "Sputter Yields of Mo, Ti, W, Al, Ag Under Xenon Ion Incidence," *European Physical Journal D*, Vol. 61, 2011, pp.587-592

43. Hu, S., Joshi, A., Khayms, V., and Smentkowski, V., Hall Thruster Plume Effects and Sputtering of Spacecraft Surfaces, 37th Joint Propulsion Conference, AIAA 2001-3356, July 9-11, 2001, Salt Lake City, UT
44. Kamhawi, H., Soulas, G., Patterson, M., and Frandina, M., "NEXT Ion Engine 2000 hour Wear Test Plume and Erosion Results," *40th AIAA/ASME/SAE/ASEE Joint Propulsion Conference and Exhibit*, AIAA 2004-3792, Ft. Lauderdale, FL, 11-14 July 2004
45. Manzella, D., et al., "Hall Thruster Plume Measurements On-Board the Russian Express Satellites," NASA/TM-2001-211217, 2001.
46. Mikellides, I.G., et al. "A Hall Effect Thruster Plume and Spacecraft Interactions Modeling Package." 27th International Electric Propulsion Conference, October 15-19, 2001, Pasadena, CA, IEPC-01-251
47. Roberts, C. and Hastings, D., "Electric Thruster Impingement Effects on Multiple Spacecraft System Environments," *38th AIAA/ASME/SAE/ASEE Joint Propulsion Conference & Exhibit*, AIAA 2002-3670, Indianapolis, IN, 7-10 July 2002
48. Young, J., Sedwick, R., Gunter, A., "Ion Sputtering Study of Spacecraft Materials in Formation Flight Regimes", publication pending
49. Young, J., Sedwick, R., "Analysis of Formation Flight Satellite Damage with respect to Electrostatic Thruster Plumes", publication pending.

Publications citing support from this grant:

1. B. Korkut, Z. Li, and D. Levin, "Three Dimensional Simulation of Ion Thruster Plumes With Octree Adaptive Mesh Refinement," IEEE Transactions on Plasma Science, March 9, 2015, Vol. 43, No. 5, May 2015, pp. 1706-1721.
2. Z. Li, A. Borner, and D. Levin, "Multi-scale study of condensation in water jets using ellipsoidal-statistical Bhatnagar-Gross-Krook and molecular dynamics modeling," The Journal of Chemical Physics, vol. 140, 224501 (2014); doi: 10.1063/1.4879797
3. Borner and D. Levin, "Coupled Molecular Dynamics, 3-D Poisson Simulations of Ionic Liquid Electrospray Thrusters, IEEE Transactions on Plasma Science, Vol. 43, Issue 1, Part, 1, 2015, (205-304), DOI: 10.1109/TPS.2014.2327913.
4. Korkut and D. Levin, "Three Dimensional Simulations of Backflows from Ion Thruster Plumes using Unstructured Grid Refinement Techniques" accepted to the Journal of Propulsion and Power, June 2016.
5. C. Loyola, J. Peralta, S.R. Broderick, K. Rajan. "Impact of extreme electrical fields on charge density distributions in alloys." *Journal of Vacuum Science and Technology*, Under Review
6. F. Vurpillot, W. Lefebvre, J.M. Cairney, C. Oberdorfer, B.P. Geiser, K. Rajan. "Advanced volume reconstruction and data mining methods in atom probe tomography." *MRS Bulletin* 41, 46-52 (2016)
7. O. Wodo, S. Broderick, K. Rajan. "Microstructural informatics for accelerating the discovery of processing-microstructure-property relationships." *MRS Bulletin* 41, 603-609 (2016)
8. S. Broderick, K. Rajan. "Extracting chemistry-property relationships by mining atom probe evaporation events." *Microscopy and Microanalysis* 22, S3 700-701 (2016)
9. K. Rajan. "Materials informatics: the materials "gene" and big data." *Annual Review of Materials Research* 45, 153-169 (2015)
10. S. Dumpala, S.R. Broderick, U. Khalilov, E.C. Neyts, A.C.T. van Duin, J Provine, R.T. Howe, K. Rajan. "Integrated atomistic chemical imaging and reactive force field molecular dynamic simulations on silicon oxidation." *Applied Physics Letters* 106, 011602 (2015)
11. S. Dumpala, D. Haley, S.R. Broderick, P.A.J. Bagot, M.P. Moody, K. Rajan. "In-situ deuterium charging for direct detection of hydrogen in vanadium by atom probe tomography." *Microscopy and Microanalysis* 21, S3 695-696 (2015)
12. S. Srinivasan, K. Kaluskar, S. Dumpala, S. Broderick, K. Rajan. "Automated voxelization of 3D atom probe data through kernal density estimation." *Ultramicroscopy* 159, 381-386 (2015)
13. S. Srinivasan, K. Kaluskar, S. Broderick, K. Rajan. "Extracting features buried within high density atom probe point cloud data through simplicial homology." *Ultramicroscopy* 159, 374-380 (2015)

14. J.M. Cairney, K. Rajan, D. Haley, B. Gault, P.A.J. Bagot, P-P. Choi, P.J. Felfer, S.P. Ringer, R.K.W. Marceau, M.P. Moody. "Mining information from atom probe data." *Ultramicroscopy* 159, 324-337 (2015)
15. S.R. Broderick, S. Dumpala, S. Padalkar, K. Rajan. "Data intensive imaging for 3D atom probe." *Microscopy and Microanalysis* 20, S3 812-813 (2014)
16. S. Dumpala, A.A. Oni, S. Padalkar, S.R. Broderick, J.M. LeBeau, K. Rajan. "Correlative imaging of stacking faults using atom probe tomography (APT) and scanning transmission electron microscopy (STEM)." *Microscopy and Microanalysis* 20, S2 996-997 (2014)
17. S. Dumpala, S.R. Broderick, P.A.J. Bagot, K. Rajan. "An integrated high temperature environmental cell for atom probe tomography studies of gas-surface reactions: instrumentation and results." *Ultramicroscopy* 141, 16-21 (2014)
18. S.R. Broderick, A. Bryden, S.K. Suram, K. Rajan. "Data mining for isotope discrimination in atom probe tomography." *Ultramicroscopy* 132, 121-128 (2013)
19. S. Broderick, J. Peralta, S. Samudrala, K. Kaluskar, B. Ganapathysubramanian, K. Rajan. "Application of computational homology and graph-theoretic approaches for quantitative chemical imaging in atom probe tomography." *Microscopy and Microanalysis* 19, S2 930-931 (2013)
20. J. Peralta, S.R. Broderick, K. Rajan. "Mapping energetics of atom probe evaporation events through first principles calculations." *Ultramicroscopy* 132, 143-151 (2013)
21. Rahnamoun, A.; van Duin, A. C. T. *Journal of Physical Chemistry A* **2014**, *118*, 2780.
22. Dumpala, S.; Broderick, S. R.; Khalilov, U.; Neyts, E. C.; van Duin, A. C. T.; Provine, J.; Howe, R.; Rajan, K. *Applied Physics Letters* **2015**, *106*, 011602.
23. Hong, S. and van Duin, A. C. T., 2015. Molecular Dynamics Simulations of the Oxidation of Aluminum Nanoparticles using the ReaxFF Reactive Force Field. *Journal of Physical Chemistry C* **119**, 17876-17886.
24. Verners, O., Psofogiannakis, G., and van Duin, A., 2015. Comparative molecular dynamics study of fcc-Al hydrogen embrittlement *Corrosion Science* **98**, 40-49.
25. Yoon, K., Ostadhossein, A., and van Duin, A. C. T., 2016. Atomistic-scale simulations of the chemomechanical behavior of graphene under nanoprojectile impact. *Carbon* **99**, 58-64.
26. Li, Z.; Borner, A.; Rahnamoun, A.; Levin, D.; van Duin, A. C. T. "BGK and MD Simulations of H_2O Supersonic Condensed Jets"; AIAA 2014, 2014, Atlanta.
27. Rahnamoun, A. and van Duin, A. C. T., 2015. Study of thermal conductivity of ice clusters after attachment to the silica surfaces using the ReaxFF reactive force field. *Phys. Chem. Chem. Phys.* **18**, 1587-1594.
28. Rahnamoun, A. and van Duin, A. C. T., 2016. Study of Ice Cluster-Amorphous Silica Collision in the Extreme Space Environment using the ReaxFF reactive force field molecular dynamics simulation method. *Journal of Applied Physics* **119**, 095901.
29. Yoon, K., Rahnamoun, A., Swett, J., Iberi, V., Cullen, I. V., Vlassiouk, I. V., Belianinov, A., Sang, X., Ovchinnikova, O. S., Rondinone, A. J., Unocic, R. R., and

van Duin, A. C. T., 2016. Atomistic-scale simulations of the defect formation in graphene under noble gas irradiation. *ACS Nano* **published online**.
30. Hong, S. and van Duin, A. C. T., 2016. Atomistic-Scale Analysis of Carbon Coating and Its Effect on the Oxidation of Aluminum Nanoparticles by ReaxFF-Molecular Dynamics Simulations. *Journal of Physical Chemistry C* **120**, 9464-9474.
31. Verners, O., Psofogiannakis, G., and van Duin, A., 2015. Comparative molecular dynamics study of fcc-Al hydrogen embrittlement *Corrosion Science* **98**, 40-49.
32. Psofogiannakis, G. and van Duin, A. C. T., 2015. ReaxFF Simulations of Hydrogen Atom Bombardment of Si,Ge, and SiGe alloy surfaces. *Surface Science* **646**, 253-260.
33. Hong, S. and van Duin, A. C. T., 2015. Molecular Dynamics Simulations of the Oxidation of Aluminum Nanoparticles using the ReaxFF Reactive Force Field. *Journal of Physical Chemistry C* **119**, 17876-17886.
34. Paupitz, R., Junkermeier, C. E., van Duin, A. C. T., and Branicio, P., 2014. Fullerenes generated from porous structures. *Phys. Chem. Chem. Phys.* **16**, 25515-25522.
35. Botari, T., Perim, E., Autreto, P. A. S., van Duin, A. C. T., Paupitz, R., and Galvao, D., 2014. Mechanical Properties and Fracture Dynamics of Silicene Membranes. *Phys. Chem. Chem. Phys.* **16**, 19417-19423.
36. Berdiyorov, G. R., Neek-Amal, M., Peeters, F. M., and van Duin, A. C. T., 2014. Stabilized nanosilicene within bilayer graphene. *Physical Review B* **89**, 024107.
37. Gouissem, A., van Duin, A. C. T., and Sharma, P., 2013. A Reactive Force Field for Zirconium and Hafnium di-Boride. *Computational Materials Science* **70**, 171-177.
38. Neyts, E. C., Ostrikov, K., Han, Z. J., Kumar, S., van Duin, A. C. T., and Bogaerts, A., 2013. Defect healing and enhanced nucleation of carbon nanotubes by low-energy ion bombardment. *Physical Review Letters* **110**, 065501.
39. Joshi, K., Raman, S., and van Duin, A., 2013. Connectivity-Based Parallel Replica Dynamics for Chemically Reactive Systems: From Femtoseconds to Microseconds. *Journal of Physical Chemistry Letters* **4**, 3792-3797.
40. Young, J.A. and R.J. Sedwick, "Sputter yields of Al surfaces under Xe ion plume impingement", *Journal of Applied Physics*, in preparation
41. Young, J.A. and R.J. Sedwick, "Sputter yields of MgF2 antireflective coating under Xe ion plume impingement", *Journal of Applied Physics*, in preparation
42. Young, J.A. and R.J. Sedwick, "Sputter yields of ITO antireflective coating under Xe ion plume impingement", *Journal of Applied Physics*, in preparation
43. Young, J.A. and R.J. Sedwick, "Photovoltaic power system degradation of spacecraft formations due to ion plume impingement", *Journal of Spacecraft and Rockets*, in preparation
44.

AFOSR Deliverables Submission Survey

Response ID:7077 Data

1.

Report Type

Final Report

Primary Contact Email

Contact email if there is a problem with the report.

acv13@psu.edu

Primary Contact Phone Number

Contact phone number if there is a problem with the report

814-8636277

Organization / Institution name

Penn State

Grant/Contract Title

The full title of the funded effort.

Tightly Coupled Mechanistic Study of Materials in the Extreme Space Environment

Grant/Contract Number

AFOSR assigned control number. It must begin with "FA9550" or "F49620" or "FA2386".

FA9550-11-1-0158

Principal Investigator Name

The full name of the principal investigator on the grant or contract.

Adrianus C. van Duin

Program Officer

The AFOSR Program Officer currently assigned to the award

Mitat Birkan

Reporting Period Start Date

09/01/2011

Reporting Period End Date

09/01/2016

Abstract

The Tightly Coupled Mechanistic Study of Materials in the Extreme Space Environment Group has worked to examine spacecraft contamination issues from the perspective of non- equilibrium gas dynamics (Levin), material response at the atomistic level (Rajan), high fidelity gas-surface chemistry models (van Duin), and experiments to characterize and test spacecraft material damage by small source ion bombardment (Sedwick). The goals of the group have been ambitious given the multi-length and time-scale facets that make this problem tremendously challenging. The length scales of contamination vary by probably twelve orders of magnitude and the variation in time scales is similar. The group has had a number of successes, described in 43 journal and conference papers that have been published or are in progress. We established collaborations across length scales, ranging from the smallest (Angstroms) to the largest scales. As such, significant progress was made in the development of computational and experimental collaborative frameworks suitable for predicting the spacecraft environment for new propellants and spacecraft materials.

Distribution Statement

This is block 12 on the SF298 form.

Distribution A - Approved for Public Release

Explanation for Distribution Statement

If this is not approved for public release, please provide a short explanation. E.g., contains proprietary information.

SF298 Form

Please attach your SF298 form. A blank SF298 can be found here. Please do not password protect or secure the PDF The maximum file size for an SF298 is 50MB.

sf0298.pdf

Upload the Report Document. File must be a PDF. Please do not password protect or secure the PDF . The maximum file size for the Report Document is 50MB.

Full_report_Oct7_2016.pdf

Upload a Report Document, if any. The maximum file size for the Report Document is 50MB.

Archival Publications (published) during reporting period:

1. B. Korkut, Z. Li, and D. Levin, "Three Dimensional Simulation of Ion Thruster Plumes With Octree Adaptive Mesh Refinement," IEEE Transactions on Plasma Science, March 9, 2015, Vol. 43, No. 5, May 2015, pp. 1706-1721.
2. Z. Li, A. Borner, and D. Levin, "Multi-scale study of condensation in water jets using ellipsoidal-statistical Bhatnagar-Gross-Krook and molecular dynamics modeling," The Journal of Chemical Physics, vol. 140, 224501 (2014); doi: 10.1063/1.4879797
3. Borner and D. Levin, "Coupled Molecular Dynamics, 3-D Poisson Simulations of Ionic Liquid Electrospray Thrusters, IEEE Transactions on Plasma Science, Vol. 43, Issue 1, Part, 1, 2015, (205-304), DOI: 10.1109/TPS.2014.2327913.
4. Korkut and D. Levin, "Three Dimensional Simulations of Backflows from Ion Thruster Plumes using Unstructured Grid Refinement Techniques" accepted to the Journal of Propulsion and Power, June 2016.
5. C. Loyola, J. Peralta, S.R. Broderick, K. Rajan. "Impact of extreme electrical fields on charge density distributions in alloys." Journal of Vacuum Science and Technology, Under Review
6. F. Vurpillot, W. Lefebvre, J.M. Cairney, C. Oberdorfer, B.P. Geiser, K. Rajan. "Advanced volume reconstruction and data mining methods in atom probe tomography." MRS Bulletin 41, 46-52 (2016)
7. O. Wodo, S. Broderick, K. Rajan. "Microstructural informatics for accelerating the discovery of processing-microstructure-property relationships." MRS Bulletin 41, 603-609 (2016)
8. S. Broderick, K. Rajan. "Extracting chemistry-property relationships by mining atom probe evaporation events." Microscopy and Microanalysis 22, S3 700-701 (2016)
9. K. Rajan. "Materials informatics: the materials "gene" and big data." Annual Review of Materials Research 45, 153-169 (2015)
10. S. Dumpala, S.R. Broderick, U. Khalilov, E.C. Neyts, A.C.T. van Duin, J Provine, R.T. Howe, K. Rajan. "Integrated atomistic chemical imaging and reactive force field molecular dynamic simulations on silicon oxidation." Applied Physics Letters 106, 011602 (2015)
11. S. Dumpala, D. Haley, S.R. Broderick, P.A.J. Bagot, M.P. Moody, K. Rajan. "In-situ deuterium charging for direct detection of hydrogen in vanadium by atom probe tomography." Microscopy and Microanalysis 21, S3 695-696 (2015)
12. S. Srinivasan, K. Kaluskar, S. Dumpala, S. Broderick, K. Rajan. "Automated voxelization of 3D atom probe data through kernal density estimation." Ultramicroscopy 159, 381-386 (2015)
13. S. Srinivasan, K. Kaluskar, S. Broderick, K. Rajan. "Extracting features buried within high density atom probe point cloud data through simplicial homology." Ultramicroscopy 159, 374-380 (2015)
14. J.M. Cairney, K. Rajan, D. Haley, B. Gault, P.A.J. Bagot, P-P. Choi, P.J. Felfer, S.P. Ringer, R.K.W. Marceau, M.P. Moody. "Mining information from atom probe data." Ultramicroscopy 159, 324-337 (2015)
15. S.R. Broderick, S. Dumpala, S. Padalkar, K. Rajan. "Data intensive imaging for 3D atom probe." Microscopy and Microanalysis 20, S3 812-813 (2014)
16. S. Dumpala, A.A. Oni, S. Padalkar, S.R. Broderick, J.M. LeBeau, K. Rajan. "Correlative imaging of stacking faults using atom probe tomography (APT) and scanning transmission electron microscopy

(STEM)." Microscopy and Microanalysis 20, S2 996-997 (2014)
17. S. Dumpala, S.R. Broderick, P.A.J. Bagot, K. Rajan. "An integrated high temperature environmental cell for atom probe tomography studies of gas-surface reactions: instrumentation and results." Ultramicroscopy 141, 16-21 (2014)
18. S.R. Broderick, A. Bryden, S.K. Suram, K. Rajan. "Data mining for isotope discrimination in atom probe tomography." Ultramicroscopy 132, 121-128 (2013)
19. S. Broderick, J. Peralta, S. Samudrala, K. Kaluskar, B. Ganapathysubramanian, K. Rajan. "Application of computational homology and graph-theoretic approaches for quantitative chemical imaging in atom probe tomography." Microscopy and Microanalysis 19, S2 930-931 (2013)
20. J. Peralta, S.R. Broderick, K. Rajan. "Mapping energetics of atom probe evaporation events through first principles calculations." Ultramicroscopy 132, 143-151 (2013)
21. Rahnamoun, A.; van Duin, A. C. T. Journal of Physical Chemistry A 2014, 118, 2780.
22. Dumpala, S.; Broderick, S. R.; Khalilov, U.; Neyts, E. C.; van Duin, A. C. T.; Provine, J.; Howe, R.; Rajan, K. Applied Physics Letters 2015, 106, 011602.
23. Hong, S. and van Duin, A. C. T., 2015. Molecular Dynamics Simulations of the Oxidation of Aluminum Nanoparticles using the ReaxFF Reactive Force Field. Journal of Physical Chemistry C 119, 17876-17886.
24. Verners, O., Psofogiannakis, G., and van Duin, A., 2015. Comparative molecular dynamics study of fcc-Al hydrogen embrittlement Corrosion Science 98, 40-49.
25. Yoon, K., Ostadhossein, A., and van Duin, A. C. T., 2016. Atomistic-scale simulations of the chemomechanical behavior of graphene under nanoprojectile impact. Carbon 99, 58-64.
26. Li, Z.; Borner, A.; Rahnamoun, A.; Levin, D.; van Duin, A. C. T. "BGK and MD Simulations of H2O Supersonic Condensed Jets"; AIAA 2014, 2014, Atlanta.
27. Rahnamoun, A. and van Duin, A. C. T., 2015. Study of thermal conductivity of ice clusters after attachment to the silica surfaces using the ReaxFF reactive force field. Phys. Chem. Chem. Phys. 18, 1587-1594.
28. Rahnamoun, A. and van Duin, A. C. T., 2016. Study of Ice Cluster-Amorphous Silica Collision in the Extreme Space Environment using the ReaxFF reactive force field molecular dynamics simulation method. Journal of Applied Physics 119, 095901.
29. Yoon, K., Rahnamoun, A., Swett, J., Iberi, V., Cullen, I. V., Vlassiouk, I. V., Belianinov, A., Sang, X., Ovchinnikova, O. S., Rondinone, A. J., Unocic, R. R., and van Duin, A. C. T., 2016. Atomistic-scale simulations of the defect formation in graphene under noble gas irradiation. ACS Nano published online.
30. Hong, S. and van Duin, A. C. T., 2016. Atomistic-Scale Analysis of Carbon Coating and Its Effect on the Oxidation of Aluminum Nanoparticles by ReaxFF-Molecular Dynamics Simulations. Journal of Physical Chemistry C 120, 9464-9474.
31. Verners, O., Psofogiannakis, G., and van Duin, A., 2015. Comparative molecular dynamics study of fcc-Al hydrogen embrittlement Corrosion Science 98, 40-49.
32. Psofogiannakis, G. and van Duin, A. C. T., 2015. ReaxFF Simulations of Hydrogen Atom Bombardment of Si,Ge, and SiGe alloy surfaces. Surface Science 646, 253-260.
33. Hong, S. and van Duin, A. C. T., 2015. Molecular Dynamics Simulations of the Oxidation of Aluminum Nanoparticles using the ReaxFF Reactive Force Field. Journal of Physical Chemistry C 119, 17876-17886.
34. Paupitz, R., Junkermeier, C. E., van Duin, A. C. T., and Branicio, P., 2014. Fullerenes generated from porous structures. Phys. Chem. Chem. Phys. 16, 25515-25522.
35. Botari, T., Perim, E., Autreto, P. A. S., van Duin, A. C. T., Paupitz, R., and Galvao, D., 2014. Mechanical Properties and Fracture Dynamics of Silicene Membranes. Phys. Chem. Chem. Phys. 16, 19417-19423.
36. Berdiyorov, G. R., Neek-Amal, M., Peeters, F. M., and van Duin, A. C. T., 2014. Stabilized nanosilicene within bilayer graphene. Physical Review B 89, 024107.
37. Gouissem, A., van Duin, A. C. T., and Sharma, P., 2013. A Reactive Force Field for Zirconium and Hafnium di-Boride. Computational Materials Science 70, 171-177.
38. Neyts, E. C., Ostrikov, K., Han, Z. J., Kumar, S., van Duin, A. C. T., and Bogaerts, A., 2013. Defect healing and enhanced nucleation of carbon nanotubes by low-energy ion bombardment. Physical Review Letters 110, 065501.
39. Joshi, K., Raman, S., and van Duin, A., 2013. Connectivity-Based Parallel Replica Dynamics for Chemically Reactive Systems: From Femtoseconds to Microseconds. Journal of Physical Chemistry Letters

4, 3792-3797.
40. Young, J.A. and R.J. Sedwick, "Sputter yields of Al surfaces under Xe ion plume impingement", Journal of Applied Physics, in preparation
41. Young, J.A. and R.J. Sedwick, "Sputter yields of MgF2 antireflective coating under Xe ion plume impingement", Journal of Applied Physics, in preparation
42. Young, J.A. and R.J. Sedwick, "Sputter yields of ITO antireflective coating under Xe ion plume impingement", Journal of Applied Physics, in preparation
43. Young, J.A. and R.J. Sedwick, "Photovoltaic power system degradation of spacecraft formations due to ion plume impingement", Journal of Spacecraft and Rockets, in preparation

New discoveries, inventions, or patent disclosures:

Do you have any discoveries, inventions, or patent disclosures to report for this period?

No

Please describe and include any notable dates

Do you plan to pursue a claim for personal or organizational intellectual property?

Changes in research objectives (if any):

Change in AFOSR Program Officer, if any:

Extensions granted or milestones slipped, if any:

A 1-year extension to September 2016 was granted.

AFOSR LRIR Number

LRIR Title

Reporting Period

Laboratory Task Manager

Program Officer

Research Objectives

Technical Summary

Funding Summary by Cost Category (by FY, $K)

	Starting FY	FY+1	FY+2
Salary			
Equipment/Facilities			
Supplies			
Total			

Report Document

Report Document - Text Analysis

Report Document - Text Analysis

Appendix Documents

2. Thank You

E-mail user

Oct 07, 2016 09:50:19 Success: Email Sent to: acv13@psu.edu